ORIGINALARBEITEN/ORIGINALS

An efficient way to calculate contact pattern movement coefficients

Andreas Fingerle[1] · Michael Otto[1] · Karsten Stahl[1]

Abstract

Planetary gearboxes are often used for their efficiency and high torque density. In large-scale wind turbine gearboxes with a rotating planet carrier, an effect called contact pattern movement was discovered where the contact pattern moves in the width direction of the mesh while the carrier rotates. A coefficient to evaluate this behavior was previously defined but its calculation requires a lot of computation time and accurate measurements can potentially be very expensive. Therefore in this publication an approach is developed to calculate an approximate contact pattern coefficient from a limited amount of data.

Effizientes Verfahren zur Berechnung von Tragbildwandernkoeffizienten

Zusammenfassung

Planetengetriebe werden oftmals wegen ihrer hohen Drehmomentdichte und hoher Effizienz eingesetzt. In großen Windenergiegetrieben mit rotierendem Planetenträger ist ein Effekt namens Tragbildwandern nachgewiesen worden, bei dem die Lastverteilung auf der Zahnflanke über einen Planetenumlauf von rechts nach links und wieder zurück wandert. Ein Koeffizient zur Bewertung dieses Verhaltens wurde bereits vorgeschlagen, allerdings ist die Bestimmung dieses Koeffizienten mittels Berechnungen oder Messtechnik bisher sehr aufwändig. In dieser Veröffentlichung wird daher ein Vorgehen beschrieben, wie ein Näherungswert für den Tragbildwandernkoeffizienten effizienter bestimmt werden kann.

1 Introduction

Planetary gears are used for various tasks where their specific advantages over helical gears outweigh the increase in complexity. These advantages, for example, lie in a high torque density, the potential for high efficiency, and a multi-shaft operation, making it possible to design compact automatic transmissions. In large-scale wind turbines, multistage planetary gearboxes are often used to increase the rotor speed to a more suitable level for the electric gen-

erator. The phenomenon of contact pattern movement was observed in these large gearboxes [1, 2]. Fig. 1 shows this effect documented in the contact between the sun and planet in different carrier positions. Contact pattern movement is rarely described in publications. However, Kamps et al. [2] developed a finite element model of a complete wind gearbox and used it to calculated the contact pattern movement in great detail. One influence they discovered was the tilting of the ring gear relative to the other central shafts in the planetary stage. Tests with contact pattern dye on the planet of a prototype gearbox imply a full contact pattern, while strain gauge measurements clearly show a moving contact pattern. This leads to the conclusion that contact pattern dye on the planet and sun contact is not a suitable method to detect contact pattern movement in planetary gearboxes (see Fig. 2).

It is possible to calculate this phenomenon with tools that consider the gearbox as a whole system to account for cross-influences between gear meshes, shafts, and bearings. While such a calculation can be performed using FEA simulations [2, 3], this approach needs a great amount of
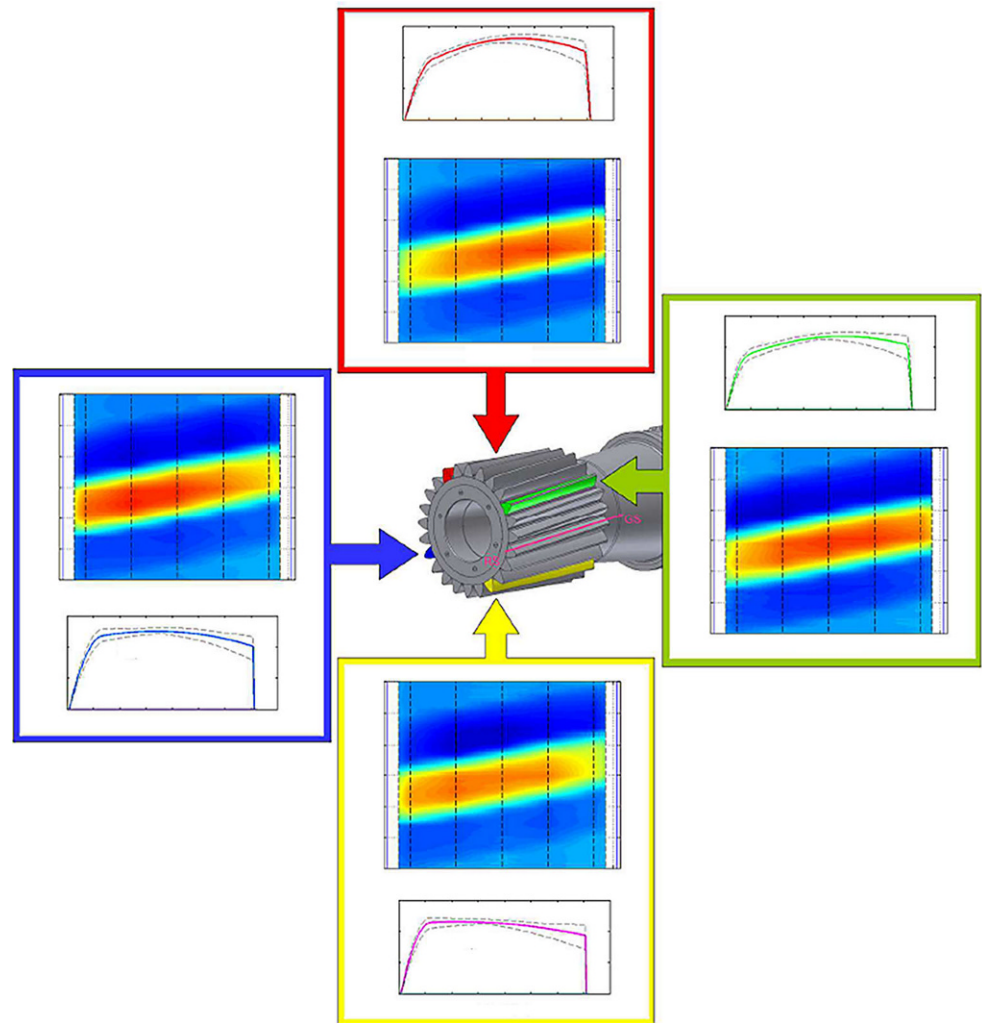
✉ Andreas Fingerle
andreas.fingerle@tum.de

Michael Otto
michael.k.otto@tum.de

Karsten Stahl
karsten.stahl@tum.de

1   Technical University Munich,
Boltzmannstrasse 15, 85748 Garching,
Germany

Fig. 1 Contact pressures and line loads of the sun-planet mesh in different angular positions of the carrier (adapted from [1])

computation time. Analytical methods are usually more efficient, such as the one used by Zhang [4], who investigated flank wear with tilted planets. In this article, the software

Fig. 2 A test with contact pattern dye implies a full contact pattern [2]

RIKOR [5–10] is used. It is an application that is continuously developed as part of research projects by the German Research Association for Drive Technology / FVA. It considers elastic deformation of teeth and shafts as well as different kind of bearings. Newer versions integrated reduced stiffness matrices to accommodate for housing and planet carrier stiffnesses. RIKOR was systematically validated with measurements in the FVA research projects FVA 592/I [11] and 592/II, RIKOR [12].

Measuring contact pattern movement is not easy as it is usually necessary to apply several tooth roots with multiple strain gauges [2, 13–15]. It is only feasible if the module is big enough for the strain gauges to fit.

Fingerle et al. [16] described a method to evaluate the contact pattern movement specifically with a single characteristic value. For this purpose they calculated the center of the area under the load distribution $x_{s,i}$ for multiple angular planet carrier positions i and called it the center of contact. They then used the difference between the extreme values
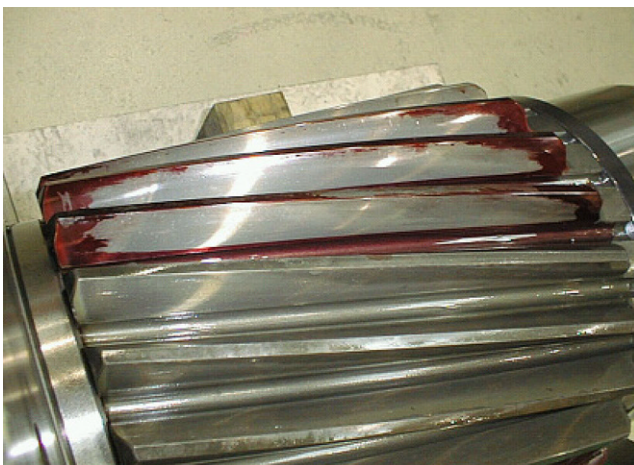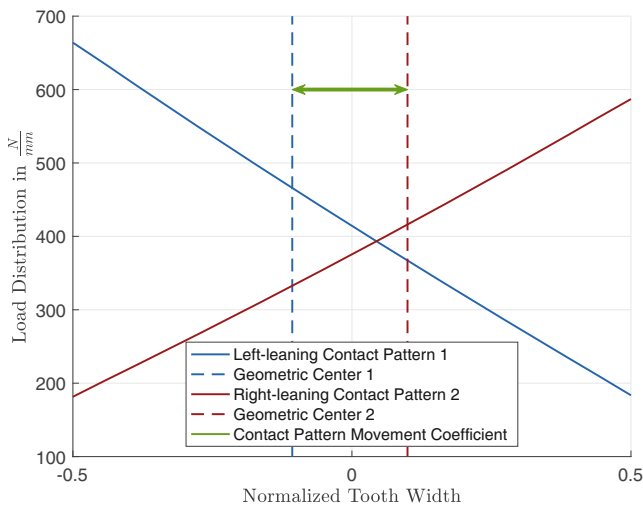
Fig. 3 Calculation of the contact pattern movement coefficient (Adapted from [16])

$x_{s,\mathrm{max}}$ and $x_{s,\mathrm{min}}$ to determine a contact pattern movement coefficient c_{CPM} as described in Eq. (1) [16].

$$c_{\mathrm{CPM}} = x_{s,\mathrm{max}} - x_{s,\mathrm{min}} \tag{1}$$

With a normalized tooth width of 1, the center of contact $x_{s,i}$ can have values between −0.5 and 0.5 and therefore the contact pattern movement coefficient lies between 0 and 1. $c_{\mathrm{CPM}} = 0$ describes no movement of the contact pattern when the carrier rotates, while $c_{\mathrm{CPM}} = 1$ is an extreme motion of the contact pattern from one tooth edge to the other.

Fig. 3 depicts this approach in a synthetic example where the bold lines show two extreme contact patterns with their center of contact respectively in dotted lines. The green double arrow shows the difference between the center of contacts, which represents the contact pattern movement coefficient c_{CPM}.

While this approach helps characterize the amount of contact pattern movement in a planetary gearbox with a single number, it can be computationally intensive to calculate this coefficient and very costly to accurately determine it via measurements. This paper aims to propose a more efficient approach to determine contact pattern movement coefficients while minimizing the loss in accuracy.

2 Determination of extreme values

The method described by Fingerle [16] depends on the knowledge of the extreme values of the center of contact within one carrier rotation. Obtaining the correct extreme values from only a few calculated or measured carrier po-

sitions is very unlikely and is therefore not a feasible approach to attain reliable and reproducible results. While calculating many carrier positions is possible, it can take considerable amounts of calculation time. Applying a large number of teeth with strain gauges to get reliable information about contact pattern movement, however, directly impacts cost. Therefore, an approach is needed to estimate a contact pattern movement coefficient from few carrier positions. To derive such an approach, the gearbox model from the calculations carried out by the author [16] is used to investigate the behavior of the center of contact when calculating small angular steps of the planet carrier rotation.

2.1 Gearbox Model

The calculations for the following investigations are performed with the analytical gearbox calculation software RIKOR L [9]. The software calculates the gearbox as a whole, which enables the consideration of cross-influences between different gear meshes and bearings. Shafts in general are represented as beam elements with consideration of the shear stress. The planet carrier is modeled as a reduced stiffness matrix to incorporate its complex stiffness behavior. Although it is possible to consider bearing compliance derived from their inner geometry, for these calculations the bearings are considered as constant stiffnesses to reduce the influence of numeric errors.

The design of the gearbox is identical to the one the authors [16] used in their earlier investigations. The general technical data are shown below in Table 1.

Fig. 4 shows a graphical representation of the gearbox model used.

The microgeometry of the teeth was determined with RIKOR calculations to have a balanced contact pattern for the case of a gearbox without deviations. Helix angle modifications were adapted for that goal and a small amount of helix crowning was added to reduce edge loads.

Table 1 Main gearbox data

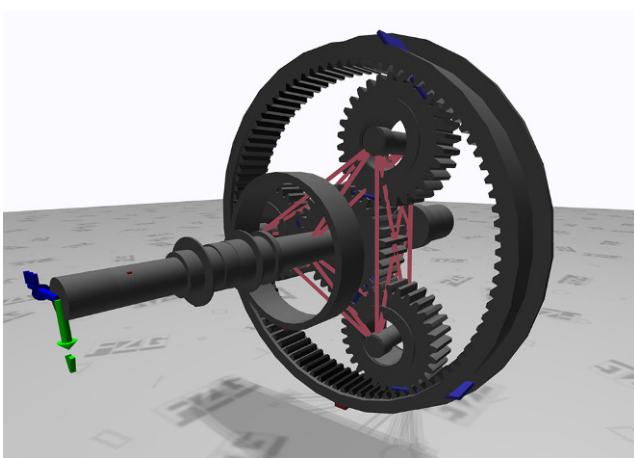| Name	Abb.	Unit	Value
Stationary gear ratio	i_0	–	−3
Gear ratio sun to carrier	i_{1s}	–	4
Number of planets	N_P	–	3
Input torque	T_{in}	Nm	900
Output torque	T_{out}	Nm	3,600
Normal module	m_n	mm	4.500
Helix angle	β	°	0
Contact ratio	ϵ_α	–	1.247
Center distance	a	mm	135.0
Common face width	b	mm	40

Fig. 4 Graphical representation of the gearbox model used

2.2 Characteristics of contact pattern movement

To determine the characteristics of the movement of the center of contact, the gearbox model is calculated with a sun shaft that is radially displaced at its bearing positions. The calculation is performed in 180 different carrier angles with a 2° increment. This approach is very computationally intensive, but it returns accurate results. Following the naming scheme of ISO norms, this most accurate approach will be called method A and the contact pattern movement coefficient will be abbreviated as $c_{\text{CPM,A}}$.

Fig. 5 shows the position of the center of contact for the three planets P1 to P3 for one carrier revolution. While the center of contact in the mesh between sun and planet moves a considerable amount, the influence on the ring gear contact is very low. Still, in both cases there is a good

correlation with harmonic oscillations. All planets essentially behave the same albeit, with the expected phase shift of 120°. These findings can now be used to derive an approach to calculate a contact pattern movement coefficient from a substitute sine curve. This approach will be called method B, with the abbreviation $c_{\text{CPM,B}}$.

2.3 Derivation of a substitute sine curve

With the time t, the amplitude A, the angular frequency ω, the vertical offset C, and the phase ϕ, the equation for a general sine oscillation reads as follows:

$$y(t) = A \cdot \sin(\omega t + \phi) + C \tag{2}$$

Because contact pattern movement from displaced central shafts happens with one oscillation per carrier rotation, the angular frequency can be set to $\omega = 1$. To determine the parameters of the sine curve there are three unknown parameters A, ϕ, and C left, which leads to a minimum of three carrier positions that need to be calculated.

Using the results y_i from three calculations, the missing parameters can be derived analytically by transforming the following Eqs. (3) to (5). For the first carrier position we assume the carrier angle to be 0° and therefore we can set $x_1 = 0$.

$$y_1 = A \cdot \sin(x_1 + \phi) + C \quad \Rightarrow \quad y_1 = A \cdot \sin(\phi) + C \tag{3}$$
$$y_2 = A \cdot \sin(x_2 + \phi) + C \tag{4}$$
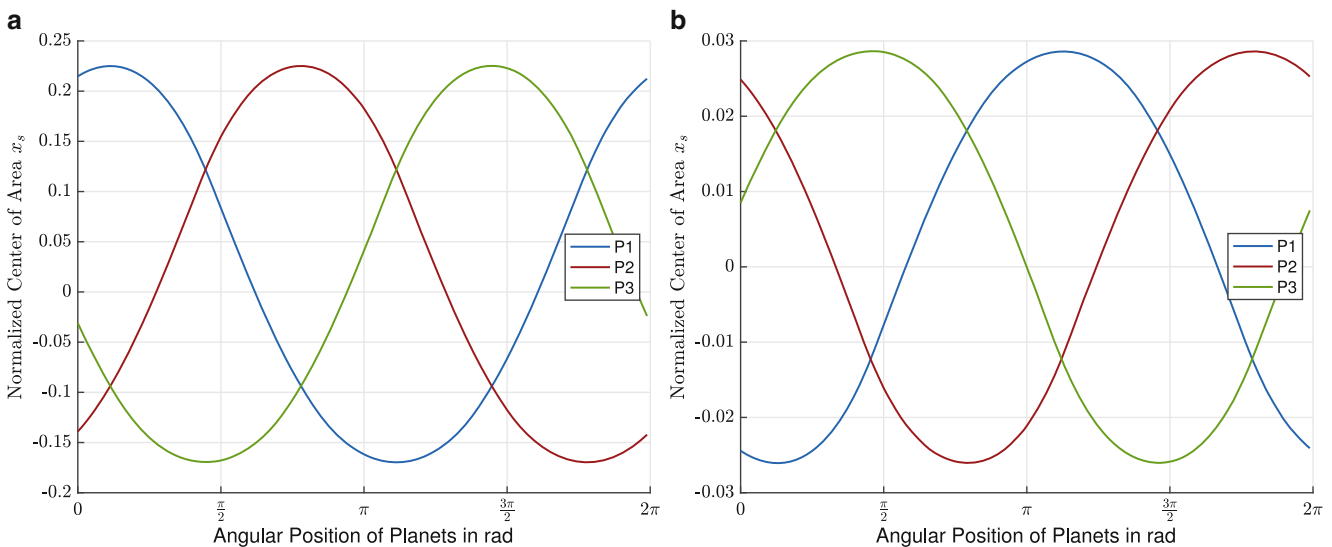$$y_3 = A \cdot \sin(x_3 + \phi) + C \tag{5}$$

Fig. 5 Movement of the center of contact over one carrier rotation (180 carrier positions). **a** Contact Sun – Planet, **b** Contact Planet – Ring gear

By transforming Eq. (3), the vertical offset C is determined, resulting in Eq. (6):

$$C = y_1 - A \cdot \sin(\phi) \tag{6}$$

Subsequently, insertion in Eq. (4) gives back the amplitude A:

$$A = \frac{y_2 - y_1}{\sin(x_2)\cos(\phi) + \cos(x_2)\sin(\phi) - \sin(\phi)} \tag{7}$$

For the complex rearrangement of Eq. (5) in terms of the phase ϕ, the MATLAB "Symbolic Math Toolbox" [17] was used. The resulting Eq. (8) for the calculation of the phase ϕ is stated below. Because of the cyclic nature of the sine curve there are infinite solutions shifted by $2 \cdot k \cdot \pi$, with k being any integer. As all values for k result in the same phase, it can be set to 0.

$$
\begin{aligned}
\phi = {} & 2 \cdot k \cdot \pi + 2 \cdot \arctan((y_3 - y_2 + (y_1^2 \cdot \cos(x_2)^2 \\
& - 2y_3^2 \cdot \cos(x_2) - 2y_2 y_3 - 2y_2^2 \cdot \cos(x_3)\phi + y_1^2 \cdot \cos(x_3)^2 \\
& + y_2^2 \cdot \cos(x_3)^2 + y_3^2 \cdot \cos(x_2)^2 + y_1^2 \cdot \sin(x_2)^2 \\
& + y_1^2 \cdot \sin(x_3)^2\phi + y_2^2 \cdot \sin(x_3)^2 + y_3^2 \cdot \sin(x_2)^2 + y_2^2 + y_3^2 \\
& - 2y_1^2 \cdot \sin(x_2) \cdot \sin(x_3) - 2y_1 y_2 \cdot \cos(x_2)\phi \\
& + 2y_1 y_2 \cdot \cos(x_3) + 2y_1 y_3 \cdot \cos(x_2) - 2y_1 y_3 \cdot \cos(x_3) \\
& + 2y_2 y_3 \cdot \cos(x_2) + 2y_2 y_3 \cdot \cos(x_3)\phi - 2y_1 y_2 \cdot \cos(x_3)^2 \\
& - 2y_1 y_3 \cdot \cos(x_2)^2 - 2y_1 y_2 \cdot \sin(x_3)^2 - 2y_1 y_3 \cdot \sin(x_2)^2\phi \\
& - 2y_1^2 \cdot \cos(x_2) \cdot \cos(x_3) + 2y_1 y_2 \cdot \cos(x_2) \cdot \cos(x_3) \\
& + 2y_1 y_3 \cdot \cos(x_2) \cdot \cos(x_3)\phi - 2y_2 y_3 \cdot \cos(x_2) \cdot \cos(x_3) \\
& + 2y_1 y_2 \cdot \sin(x_2) \cdot \sin(x_3) + 2y_1 y_3 \cdot \sin(x_2) \cdot \sin(x_3)\phi \\
& - 2y_2 y_3 \cdot \sin(x_2) \cdot \sin(x_3))^{\frac{1}{2}} + y_1 \cdot \cos(x_2) - y_1 \cdot \cos(x_3) \\
& + y_2 \cdot \cos(x_3) - y_3 \cdot \cos(x_2))\phi / (y_1 \cdot \sin(x_2) - y_1 \cdot \sin(x_3) \\
& + y_2 \cdot \sin(x_3) - y_3 \cdot \sin(x_2)))
\end{aligned}
\tag{8}
$$

Now that all unknown parameters were defined, the sine curve can be used to determine characteristic values of the center of contact. While the vertical offset C shows the average center of contact and therefore indicates how one-sided the contact is in general, the contact pattern movement coefficient can be deduced from the amplitude of the oscillation:

$$c_{\text{CPM,B}} = 2 \cdot A \approx c_{\text{CPM,A}} \tag{9}$$

Table 2 Calculated variants

Designation	Feature
a	Radially displaced sun shaft
b	Radially displaced planet carrier
c	Tilted planet carrier
d	Tilted ring gear

3 Validation of the approach

To validate the approach, four different variants of the gearbox that are known to show contact pattern movement are calculated using the methods A and B. As before, with method A, 180 carrier positions are calculated with an angle increment of 2°. For method B, three carrier positions with an increment of 120° are calculated, starting with an angle of 0° which matches the position of the gearbox shown in Fig. 4. Table 2 shows the different variants. All displacements are acting on the bearing positions. The ring gear is modeled as being fixed to the inertial system on both sides of the mesh.

Fig. 6 shows the course of the center of contact for all variants in the mesh between sun and planet P1 as a qualitative comparison of the two methods. The blue lines show the 180 carrier positions of method A with linear interpolation between the calculated points. The sine curve derived from three carrier positions using the equations shown in Sect. 2.3 is displayed in red. For all variants, the substitute sine curves show a strong similarity with the course of the center of contact calculated with method A.

The comparison in Fig. 7 depicts the course of the center of contact in the mesh between ring gear and planet. It also shows a sine-like shape although it differs slightly more from an ideal sine curve than is the case in the sun contact. In particular, the variant **b** with the radially displaced planet carrier stands out, which results in a greater difference between methods A and B. The maximum deviation of the other variants **a**, **c**, and **d** is considerably lower. Variant **c** being the only considered variant where the method B value is lower than that of method A.

In a qualitative comparison the sine curves derived from method B show similar behavior to the more detailed method A approach. However, because there are deviations from ideal sine curves and only three points are calculated with a 120° delta, it is to be expected that the initial angle has an effect on the calculated sine curve parameters. Therefore a study is performed to investigate the influence of the initial planet carrier position on the calculated contact pattern movement coefficient and thereby determine the validity of the approach. In this study the starting angle of the planet carrier was varied from 0° in 180 positions with an increment of 2° covering a full circle. The calculation was performed for each of the four variants and the
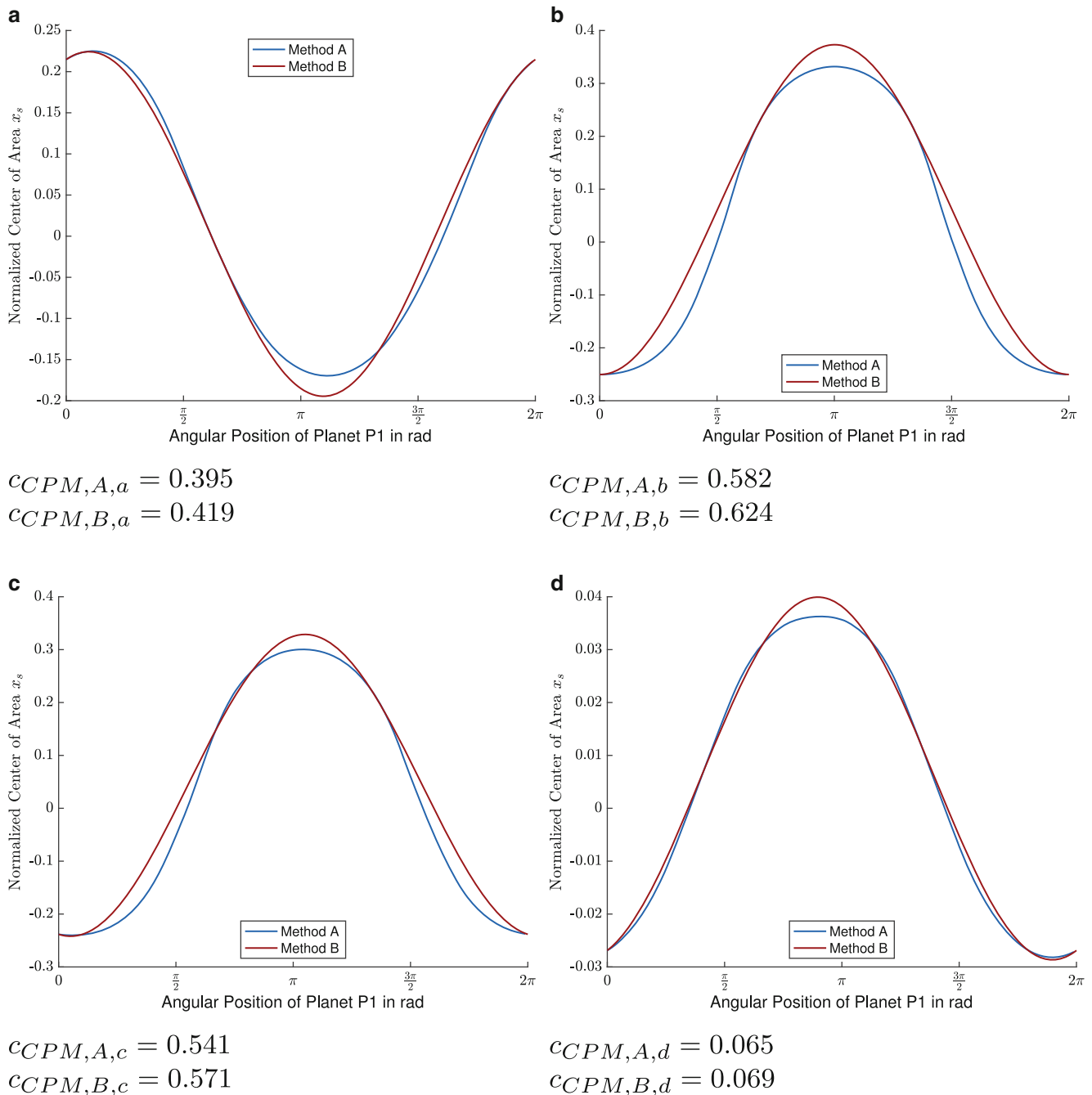
$$c_{CPM,A,a} = 0.395$$
$$c_{CPM,B,a} = 0.419$$

$$c_{CPM,A,b} = 0.582$$
$$c_{CPM,B,b} = 0.624$$

$$c_{CPM,A,c} = 0.541$$
$$c_{CPM,B,c} = 0.571$$

$$c_{CPM,A,d} = 0.065$$
$$c_{CPM,B,d} = 0.069$$

Fig. 6 Comparison of contact pattern movement in the sun contact calculated with methods A and B. **a** Radially displaced sun, **b** Radially displaced planet carrier, **c** Tilted planet carrier, **d** Tilted ring gear

resulting $c_{CPM,B}$-values were recorded. Fig. 8 shows the resulting graphs for the sun and ring gear mesh with linear interpolation between the calculated points.

It can clearly be observed that the initial carrier angle has an influence on the calculated sine curve and therefore the derived contact pattern movement coefficient. In general the absolute deviation is greater for curves that are less similar to an ideal sine curve, like it is the case with variant **c** in the ring gear contact. Table 3 summarizes the resulting mean

$c_{CPM,B}$-values as well as the differences between methods A and B and maximum deviations.

The results show that in every investigated variant the presence of contact pattern movement is clearly detectable. There are relative differences between the mean $c_{CPM,B}$-values and the method A results of up to 20.8 % and a maximum deviation of 33.5 %, however the higher relative deviations only occur in cases with low contact pattern movement coefficients and therefore the absolute differences are
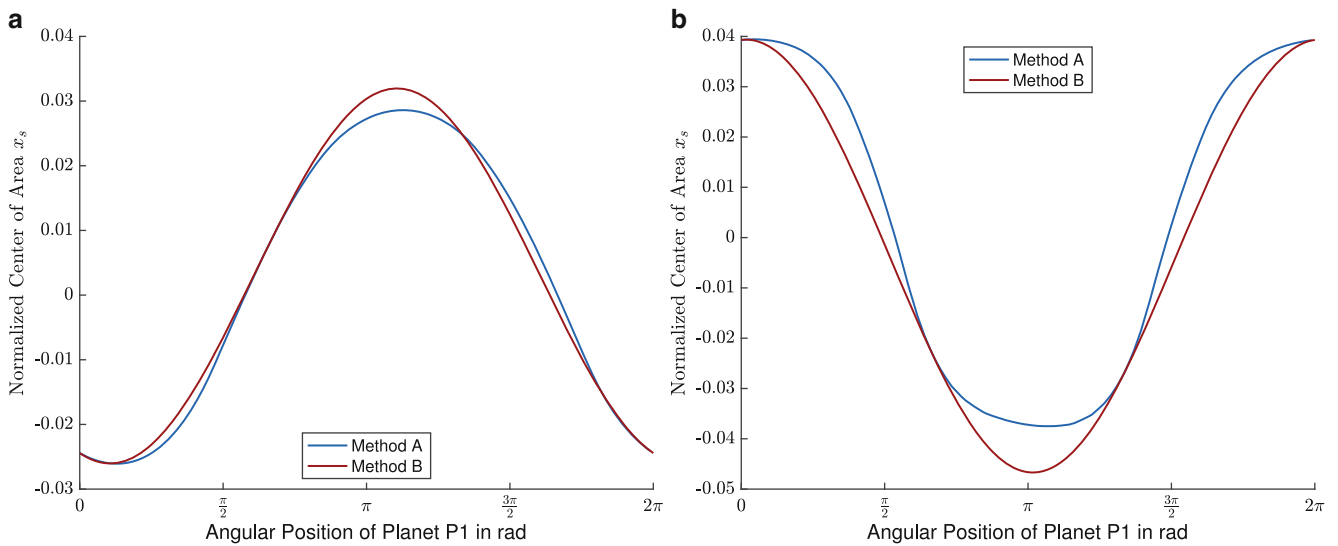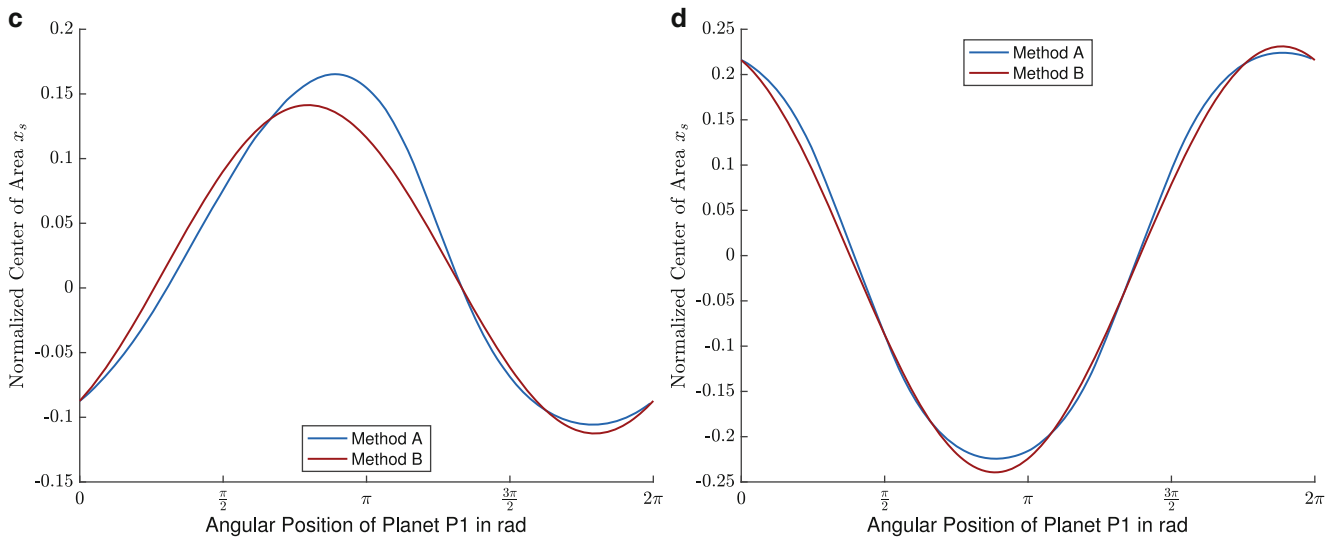
$$c_{CPM,A,a} = 0.055$$
$$c_{CPM,B,a} = 0.058$$

$$c_{CPM,A,b} = 0.077$$
$$c_{CPM,B,b} = 0.086$$

$$c_{CPM,A,c} = 0.271$$
$$c_{CPM,B,c} = 0.254$$

$$c_{CPM,A,d} = 0.449$$
$$c_{CPM,B,d} = 0.471$$

Fig. 7 Comparison of contact pattern movement in the ring gear contact calculated with methods A and B. **a** Radially displaced sun, **b** Radially displaced planet carrier, **c** Tilted planet carrier, **d** Tilted ring gear

also low. In cases with significant contact pattern movement ($c_{CPM,A} > 0.1$) the relative difference from the mean method B value to the method A value stays below 10 % while the maximum deviation is lower than 15 % which should be an acceptable error for most applications.

4 Conclusion

This publication proposes a calculation approach to determine a contact pattern movement coefficient based on Fingerle [16] from a limited set of calculated or measured angular carrier positions. With three carrier positions, a substitute sine curve can be determined which can then be used to approximate a contact pattern movement coefficient without a significant loss in accuracy. This approach can be
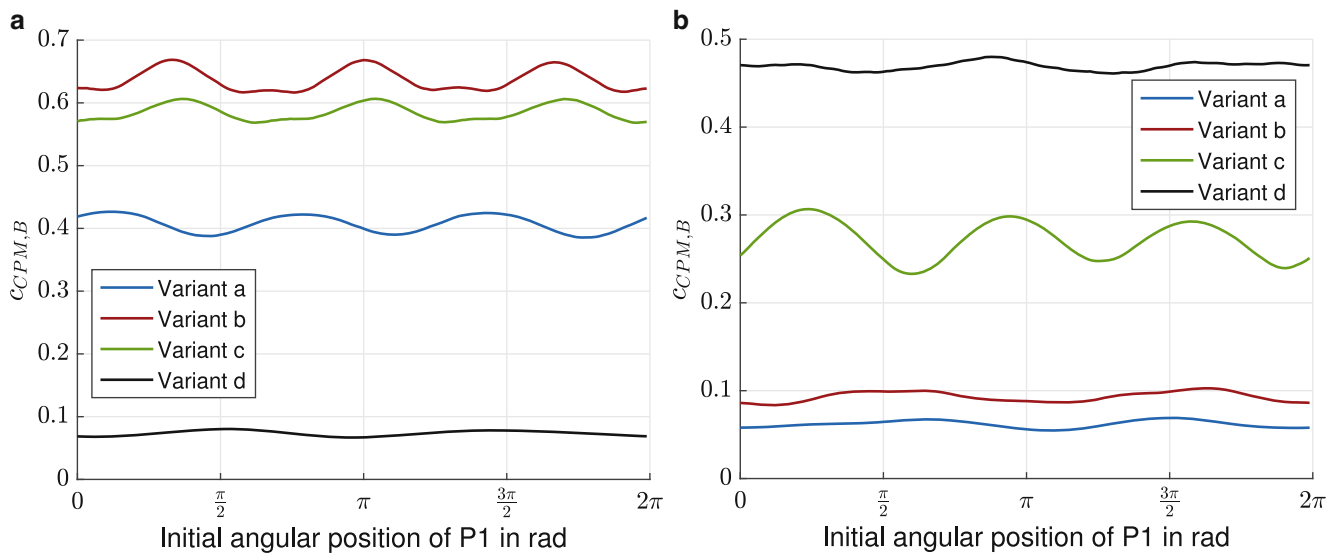
a

b

Fig. 8 Method B coefficients for varying starting angles. **a** Contact Sun – Planet, **b** Contact Planet – Ring gear

Table 3 Differences between methods A and B

Mesh	Variant	$c_{CPM,A}$	Mean $c_{CPM,B}$	Difference between $c_{CPM,A}$ and the mean $c_{CPM,B}$ in percent	Max. deviation from $c_{CPM,A}$ in percent
Sun – planet	a	0.395	0.407	3.04	8.00
	b	0.582	0.637	9.45	14.94
	c	0.541	0.585	8.13	12.14
	d	0.065	0.074	13.85	23.53
Planet – ring gear	a	0.055	0.062	12.27	25.27
	b	0.077	0.093	20.78	**33.51**
	c	0.271	0.271	0.00	14.10
	d	0.449	0.469	4.45	6.90

used to considerably reduce computation time or reduce the number of strain gauges needed for measurements. The examples calculated to verify the approach show that it is a suitable method to detect the presence of contact pattern movement with low computational effort. One influence on the accuracy of the method is the shape of the curve and how it differs from an ideal sine curve. For future studies it should be investigated which parameters influence the shape of the curve and cause these deviations from an ideal sine curve. Furthermore, different curve fitting methods with more than three calculated points could be investigated to determine the best trade-off between calculation time and accuracy. However, especially for the analysis of measurements, where additional strain gauges have direct impact on cost, the proposed approach with three measured positions should be adequate in most practical applications. For scientific investigations method A should be preferred for highest accuracy.

References

1. Leimann D (2013) Evolution in gear micro-geometry design for wind turbine gearboxes with respect to load distribution and noise and vibrations. VDI Wissensforum.
2. Kamps A, Klein-Hitpass A (2015) Einfluss von elastischen Verformungen auf die Auslegung und den Betrieb von Getrieben für Windkraftanlagen. Dresdner Maschinenelemente Kolloquium.
3. Bodas A, Kahraman A (2004) Influence of carrier and gear manufacturing errors on the static load sharing behavior of planetary gear sets. JSME Int J Ser C 47(3):908–915. https://doi.org/10.1299/jsmec.47.908
4. Zhang J, Wang T, Chen T (2018) The effect of axis misalignment on gear wear in planetary gear trains. In: Institut National des Sciences Appliquees (ed) International Gear Conference 2018. Chartridge Books, Oxford, pp 1066–1078
5. Placzek, T (1988) Lastverteilung und Flankenkorrektur in gerad- und schrägverzahnten Stirnradstufen. Dissertation, Technische Universität München, Munich
6. Neubauer B, Otto M, Stahl K (2015) Efficient calculation of load distribution and design of tooth flank modifications in planetary gear systems: Static load and deformation analysis in a fully coupled mechanical model of a gear box structure with laplasn. In: VDI (ed) International Conference on Gears 2015, vol 1, pp 549–558
7. Weinberger U, Glenk C (2017) FVA Heft Nr. 1250 – Einbindung elastischer Gehäusestrukturen in die Getriebeauslegung mit RIKOR und Visualisierung des Getriebegesamtsystems in der FVA-Workbench. Forschungsvereinigung Antriebstechnik e.V., Frankfurt/Main
8. Fingerle A, Hein M, Tobie T, Otto M, Stahl K (2019) Methode zur Auslegung von Verzahnungskorrekturen unter Lastkollektivbelastung. Konstruktion 71:76–81. https://doi.org/10.37544/0720-5953-2019-09-76
9. Weinberger U, Otto MK, Stahl K (2019) Closed-form calculation of lead flank modification proposal for spur and helical gear stages. J Mech Des. https://doi.org/10.1115/1.4045396
10. Schweigert D, Weinberger U, Otto M, Stahl K (2022) Advanced method of including housing stiffness into calculation of gear systems. Forsch Ingenieurwes 86(2):231–248. https://doi.org/10.1007/s10010-022-00585-z
11. Fürstenberger M (2011) FVA Heft Nr. 987 – Validierung RIKOR: Validierung und Untersuchung von Anwendungsgrenzen des FVA Getriebeprogramms RIKOR anhand von Verformungsmessungen: Forschungsvorhaben Nr. 592 I. Forschungsvereinigung Antriebstechnik e.V., Frankfurt/Main
12. Daffner M (2017) FVA-Heft Nr. 1232 – Validierung RIKOR: Weiterführende Validierung der Verformungsrechnung in RIKOR – Detaillierte Betrachtung Einzelner Getriebeelemente: Forschungsvorhaben Nr. 592 II. Forschungsvereinigung Antriebstechnik e.V., Frankfurt
13. Kahraman A (1999) Static load sharing characteristics of transmission planetary gear sets: Model and experiment. SAE Technical Papers (1999-01-1050), pp 233–241
14. Nam JS, Park YJ, Han JW, Nam YY, Lee GH (2016) The effects of non-torque loads on a three-point suspension gearbox for wind turbines. Int J Energy Res 40(5):618–631. https://doi.org/10.1002/er.3373
15. Terrin A, Conte LF, Meneghetti G (2018) Experimental evaluation of tooth-root bending strains of a sund gear in a planetary gear set for off-highway axles. In: Institut National des Sciences Appliquees (ed) International Gear Conference 2018, vol 2. Chartridge Books, Oxford, pp 1079–1088
16. Fingerle A, Otto M, Stahl K (2020) Definition of a coefficient to evaluate a moving contact pattern in planetary gearboxes. Forsch Ingenieurwes 84(3):235–243. https://doi.org/10.1007/s10010-020-00405-2
17. The MathWorks Inc MATLAB R2020b (version 9.9.0.1467703), Natick, MA, USA (2020). https://de.mathworks.com/help/matlab/. Accessed 2021-04-27